Research Paper

PAIN®

OPEN

Unbiased analysis of the dorsal root ganglion after peripheral nerve injury: no neuronal loss, no gliosis, but satellite glial cell plasticity

Annemarie Schulte[a], Hannah Lohner[b], Johannes Degenbeck[b], Dennis Segebarth[c], Heike L. Rittner[b,*], Robert Blum[a], Annemarie Aue[b]

Abstract

Pain syndromes are often accompanied by complex molecular and cellular changes in dorsal root ganglia (DRG). However, the evaluation of cellular plasticity in the DRG is often performed by heuristic manual analysis of a small number of representative microscopy image fields. In this study, we introduce a deep learning–based strategy for objective and unbiased analysis of neurons and satellite glial cells (SGCs) in the DRG. To validate the approach experimentally, we examined serial sections of the rat DRG after spared nerve injury (SNI) or sham surgery. Sections were stained for neurofilament, glial fibrillary acidic protein (GFAP), and glutamine synthetase (GS) and imaged using high-resolution large-field (tile) microscopy. After training of deep learning models on consensus information of different experts, thousands of image features in DRG sections were analyzed. We used known (GFAP upregulation), controversial (neuronal loss), and novel (SGC phenotype switch) changes to evaluate the method. In our data, the number of DRG neurons was similar 14 d after SNI vs sham. In GFAP-positive subareas, the percentage of neurons in proximity to GFAP-positive cells increased after SNI. In contrast, GS-positive signals, and the percentage of neurons in proximity to GS-positive SGCs decreased after SNI. Changes in GS and GFAP levels could be linked to specific DRG neuron subgroups of different size. Hence, we could not detect gliosis but plasticity changes in the SGC marker expression. Our objective analysis of DRG tissue after peripheral nerve injury shows cellular plasticity responses of SGCs in the whole DRG but neither injury-induced neuronal death nor gliosis.

Keywords: Dorsal root ganglia, Satellite glial cell activation, Bioimage segmentation, Deep learning, Neuropathic pain

1. Introduction

Nerve lesions and subsequent neuropathic pain often occur after trauma, surgery, or accidents and cause cellular plasticity changes in the dorsal root ganglia (DRG). Affected sensory neurons in the DRG are the first relay centers for transmission and processing of peripheral nociceptive sensory signals.[21] The function of DRG neurons depends on satellite glial cells (SGCs), which are tightly wrapped around the neuronal cell bodies of the DRG, so that each neuron represents an electrical and anatomical unit.[24,48,49,58] Glutamine synthetase (GS) is often used as a selective immunohistochemical marker,[23,27,41] although only 60% of SGCs express GS in rodents.[1–3] The glial fibrillary acidic protein (GFAP) is a typical reactivation marker for SGCs in rats.[24,43,61]

Nerve injury causes adaptations in the DRG cell composition. For instance, neuronal loss is seen after sciatic nerve axotomy, at least in some animal models.[33] Satellite glial cells are activated after ventral root avulsion,[65] nerve transection,[36,61] chronic constriction injury,[47] partial nerve ligation,[63] spared nerve injury (SNI), and spinal nerve ligation.[37,62] As early as 2 to 3 d after nerve injury, SGCs as well as macrophages proliferate and change their expression profile.[17,27,32,65] After SNL, GFAP starts to be upregulated after 4 hours and peaks at day 7.[37] In comparison, GFAP upregulation after SNI seems to be less pronounced.[62] SGC plasticity after injury might contribute to neuropathic pain by increasing neuronal activity.[24,30] Furthermore, SGCs might even acquire neural progenitor–like properties, opening a starting point for regenerative medicine.[15,46]

Most studies use immunofluorescence microscopy to analyze the DRG after peripheral nerve injury.[5,44,60,62] However, analysis of the corresponding bioimages often relies on the individual criteria of the human expert looking at the images and annotating corresponding image features. This heuristic method is relatively complex, labor intensive, creates a high level of subjectivity, and creates a highly varying interrater agreement on the same bioimages.[19] Furthermore, for analyzing the DRG, it is virtually

Sponsorships or competing interests that may be relevant to content are disclosed at the end of this article.

[a] Department of Neurology, University Hospital of Würzburg, Würzburg, Germany, [b] Department of Anesthesiology, Center for Interdisciplinary Pain Medicine, Intensive Care, Emergency Medicine and Pain Therapy, University Hospital of Würzburg, Würzburg, Germany, [c] Institute of Clinical Neurobiology, University Hospital of Würzburg, Würzburg, Germany

**Corresponding author. Address: Department of Anesthesiology, Intensive Care, Emergency and Pain Medicine, Center for Interdisciplinary Pain Medicine, University Hospital of Würzburg, Würzburg, Germany. Tel.: +49 931 201-30251; fax: +49 931 201-30259. E-mail address: Rittner_H@ukw.de (H. Rittner).*

Supplemental digital content is available for this article. Direct URL citations appear in the printed text and are provided in the HTML and PDF versions of this article on the journal's Web site (www.painjournalonline.com).

PAIN 164 (2023) 728–740

http://dx.doi.org/10.1097/j.pain.0000000000002758

impossible to blind experimenter's rating behavior because plasticity changes are visible for the expert.

To ensure greater objectivity in bioimage analysis, many open-source deep learning (DL)–based algorithms have been optimized for image recognition tasks.[39] They enable an automated large-scale image analysis process while being more objective, valid, and reliable than a single human expert.[56] Although DL has become one of the gold standards for bioimage analysis, the complexity and lack of widely accepted benchmarks and training data sets hinders a wide usage.[34,42]

Here, we worked out a strategy for systematic, objective analysis of pain-related cellular plasticity changes in the DRG. The strategy allows unbiased analysis of large-field bioimages of whole DRG sections. Applying our DL-based approach confirms a widely observed injury effect, GFAP upregulation in SGCs in rats. Furthermore, SGCs undergo phenotype changes close to their sensory neuron soma. Notably, we could not see controversially discussed plasticity changes like injury-related neuronal death or gliosis.

2. Materials and methods

2.1. Animals

Male Wistar rats (Janvier labs, Le Genest-St-Isle, France) aged 4 weeks and weighing 125 to 150 g were cage housed, 6 in each, with enrichment tools in a circadian light rhythm (12 /12 hours light/dark cycle, 21-25°C, 45-55% humidity) with water and food ad libitum. Because the described methodological aspects were independent of gender, we did not use female rats. Animal protocols (# REG 2-733) have been approved by the animal care committee of the Regierung von Unterfranken, Würzburg, Germany. All procedures were in accordance with international guidelines for the care and use of laboratory animals (EU Directive 2010/63/EU for animal experiments).

2.2. Sciatic nerve injury

Rats were randomly divided into SNI surgery and sham control groups holding animals of each group in a cage 1 week for habituation. Animals underwent surgery under deep anesthesia with isoflurane (1.8 vol%, fiO2). To expose the sciatic nerve with its 3 branches, the skin was incised. The common peroneal and the tibial nerve were loosely ligated with 4-0 vicryl and a piece of approximately 3 mm was cut out of the ligation site, although the sural nerve remained intact.[6,9] In the sham animals, the sciatic nerve was exposed, but the common peroneal and the tibial nerve were not cut. Surgery was performed unilaterally, and in the following experiments, the hind paw with SNI or sham surgery was designated as ipsilateral (IL) and the control paw as contralateral (CL).

2.3. Behavioral testing

Behavioral tests were performed by the same tester at the same time one day before (baseline; BL) and on days 2, 4, 7, 10, and 14 after SNI or sham surgery. Mechanical allodynia, cold, allodynia, and heat hyperalgesia were all evaluated on the same day at 30-minute intervals.

Mechanical sensitivity was determined using the von Frey test.[4,8,50,53] Rats were placed separately on a wire mesh in transparent plastic cages for 20 minutes every other day for one week to practice handling and to habituate rats to the environment. Before testing, rats were put on the wire mesh into the cages for 10 minutes to ensure habituation. The von Frey filaments (Stoelting Co, Thermo) ranging from 1 g to 15 g were applied to the lateral plantar surface of each hind paw. A positive response was marked by the withdrawal of the paw. Three trials were performed on each hind paw starting with the contralateral side (2 minutes break between each stimulus presentation). Dixon's up and down method was used to calculate the 50% von Frey filament paw withdrawal threshold response.[10]

To detect cold allodynia, rats were tested using the acetone assay. A small drop of acetone was applied to the lateral plantar surface of the hind paw, and the response to the stimulus was observed for 20 seconds. The response score ranged from 0 to 3: 0, no response; 1, brisk withdrawal or flick of the paw; 2, repeated flicking of the paw; 3, repeated flicking and licking of the paw.[13,64] Acetone was applied 3 times to each rat starting with the contralateral hind paw. A 5-minute interval was set between each stimulus.

Sensitivity to heat was determined with the Hargreaves test (IITC plantar test apparatus model 400 heated base).[22,25] Rats were placed in cages on a glass floor, and the plantar surface of the hind paw was exposed to a radiant heat beam for a maximum of 20 seconds. The time until paw withdrawal was recorded, and the latency was calculated after 2 trials for each hind paw with a 5-minute interval.

2.4. Perfusion and tissue processing

Animals were harvested 7 or 14 d after SNI/sham surgery. First, rats received deep anesthesia with isoflurane and were perfused intracardially with phosphate buffered saline (PBS) enriched with 0.4% heparin (approximately 100 mL). After clearing organs from blood, the buffer solution was changed to 4% paraformaldehyde (PFA, pH 7.4). A successful fixation was indicated by spontaneous movement and stiffness of the rat body.[14] Ipsilateral and contralateral L4 and L5 DRG were dissected and postfixed with 4% PFA for 30 minutes, quenched with Tris-buffered glycine (100 mM) for 1 hour, washed 3 times, and cryoprotected in 30% sucrose in PBS overnight. Dorsal root ganglia samples were marked with a number to blind the examiner, embedded at different angles in Tissue Tek O.C.T. Compound (Sakura Finetek Europe B.V., AV Alphen aan den Rijn, The Netherlands) to visualize the DRG from different sides, and snap frozen in liquid nitrogen. The samples were processed as quickly as possible and stored at −80°C.

2.5. Immunofluorescence

Serial sections (collecting every 10th slice in sequential order) of 16-μm thickness were cut at −30°C in a cryostat (Leica Biosystems CM3050 S Research Cryostat, Leica Biosystems Nussloch GmbH, Nussloch, Germany). Due to different angled DRG embedding, 2 to 13 section per DRG were collected. Slides were quenched with Tris-buffered glycine for 15 minutes and blocked with 10% donkey serum in 0.3% Triton X-100 for 1hour at room temperature. Slides were costained with primary antibodies in 10% donkey serum in PBS overnight at 4°C: chicken Neurofilament, Heavy (NF-H) antibody (1:8000, EMD Millipore, number AB5539; RRID: AB_11212161), rabbit GFAP antibody (1:1000, OriGene Technologies, Rockville, MD, number DP014; RRID: AB_1001789), and mouse GS antibody (1:200, BD Biosciences, Franklin Lakes, NJ, number 610517; RRID: AB_397879). After washing in PBS, slides were incubated with secondary antibodies in 10% donkey serum for 1 hour at room temperature. For NF-H, Alexa fluor 488 donkey antichicken antibody (1:500, Jackson Immuno Research, West Grove, PA, number 703-545-155; RRID: AB_2340375); for GFAP, Cy3 donkey antirabbit antibody (1:500, Jackson Immuno Research,

West Grove, PA, number 711-165-152; RRID: AB_2307443); and for GS, Cy5 donkey antimouse antibody (1:500; Jackson Immuno Research, West Grove, PA, number 715-175-150; RRID: AB_2340819). After washing, DAPI was used to stain nuclei, and the sections were mounted with Aqua-Poly/Mount (Polysciences, Inc, Warrington, PA).

2.6. Microscopy and quantitative image analysis

Imaging of the immunofluorescence-labeled serial sections was performed with the same settings for each antibody using large-field (tile) microscopy with a 20x/0.8M27 objective (Axio Imager 2, Zeiss, Jena, Germany). Depending on size and orientation, images of 2 to 13 sections per rat DRG with a resolution of 0.908 μm/pixel were acquired. As there was a 160-μm distance between each serial section, double counting of cells was avoided.

For image feature segmentation, we followed guidelines for reproducible DL-based bioimage analysis.[56] Automated image segmentation was performed with the DL pipeline *deepflash2*.[19] During preprocessing, images were converted from the Zeiss czi file format to tiff files using python. Annotation was performed on 15 exemplary images for each marker by 3 experts using ImageJ.[54] With an ImageJ macro, regions of interest (ROIs) were converted to binary masks. For ground truth estimation, the simultaneous truth and performance level estimation (STAPLE) method provided in the *deepflash2* GUI was used. The data set was split into 80% training and 20% testing data set, so that 12 neurofilament (NF) images and masks were used to train consensus models for neurons and 24 GS and GFAP images and mask to train consensus models for ring-shaped glial cells. Three consensus DL models were trained to form a model ensemble. The model performance was tested by calculating the Jaccard similarity coefficient score, also called intersection over union (IoU), to compare the prediction labels with the annotated labels of the test data set (Supplementary Table 1, available at http://links.lww.com/PAIN/B703). The IoU is defined as the size of the intersection divided by the size of the union of 2 sets of pixels (A, B): $M_{IoU}(A, B) := \frac{|A \cap B|}{|A \cup B|}$.

The model ensembles were applied on all acquired images and segmentation quality was verified by the test dataset and by skimming over the images. NF images of rat 4 to 6 7 days after SNI needed to be adjusted in brightness and contrast. Dorsal root ganglia images and masks are openly available.[55]

Consecutive analysis of the segmented images was programmed in python. Tissue area was defined by thresholding the NF images using the Li thresholding method[35] and further dilating and eroding the resulting mask. For parameters regarding the size of neurons, only neurons bigger or equal 202 μm^2 were included because this was the smallest neuron size annotated. Because of the proximity of SCG to neurons, we introduced a new parameter, the percentage of neurons in proximity to GFAP/GS-positive glial cells, to assign SGCs to their corresponding neuron. To this end, both the NF mask and the glial cell mask were dilated by one pixel. If the overlap between a dilated neuron and the surrounding glial cell mask was bigger than 0, the neuron was counted. The parameters were calculated for each image and then averaged for each DRG. For further details, see https://github.com/AmSchulte/DRG.

2.7. Recommendations for the praxis

2.7.1. Image acquisition

For adaptations across projects, we recommend acquiring tile images at the same resolution. Within a project, image acquisition criteria should be kept constant (objective, intensity of excitation light with a stable LED, exposure time, bit range, binning, and gain setting of the camera). It can happen that the experimenter must adapt the image acquisition condition, for instance, to avoid pixel saturation or because of insufficient labelling. We found that DL models can still reliably extract the image features, but only when the models are trained on the whole variety of existing images. In case of very strong differences in signal intensity between experimental conditions, we recommend making 2 images. The first image should avoid pixel saturation in the signal of interest. The second image should prioritize the "weaker" signal, which might cause pixel saturation in the brighter signals, eg, because of longer image acquisition time or higher excitation light intensity.

2.7.2. Readaptation to a new project

Adaptation of the approach to other pathology-induced changes would need the development of new DL models. For data organization, computational adaptations, and recalibration to other image features, we calculate less than a workweek. We recommend using 3 experts and 10 to 15 images for object annotation. Typically, this takes 5 to 8 hours per expert, depending on the complexity of the image feature. Models need to be trained on the whole variety of existing images. Model training (computational time ~ 30 minutes) and prediction of the segmentations can be computed in one day on a local, GPU-equipped PC, for hundreds of tile-scan images and thousands upon thousands of image features. After adaptation, new data or similar image features can be analyzed with the same workflow in 1 to 2 days. For a fast, a priori test trial, 2 annotated images are sufficient: one for DL model training and one for validation.

2.7.3. Feature counting and intensity measures

Deep learning–based segmentation allows extraction of intensity values from single ROIs. The huge amount of intensity measures can enable statistical detection of effects and can be used for clustering of cell phenotypes (eg, expression level changes in subtypes of sensory neurons). Notably, the DL system accepts considerable variability in the raw images. Variability is typically caused by changes in slice quality (eg, after storage of tissue material), variations in the labelling quality, or intensity changes for biological reasons (eg, changes in signal-to-noise ratios between the image feature and the surrounding tissue under experimental conditions). Image feature counting is a conservative measure and provides solid results, even in data with high variability. We recommend looking at both, intensity measures (mean intensity, integrated density in ROIS) as well as image feature counting.

2.8. Statistical analysis

For the mechanical and thermal nociceptive thresholds, statistical significance was tested using the one-way analysis of variance followed by Tukey post hoc test for multiple comparisons. All graphs represent means ± SEM. The significance level was set at $P < 0.05$ ($^*P < 0.05$; $^{**}P < 0.01$; $^{***}P < 0.001$). Analyses were performed with GraphPad Prism 9 software.

Image quantifications were tested for significance using python. First, each data group was tested for normal distribution with the Shapiro test. If the data were not normal distributed, the Kruskal–Wallis H-test and post hoc Mann–Whitney rank test was performed. Normally distributed data were tested for equal variance with the Bartlett test. Data with unequal variance were tested with the Alexander Govern test, data with equal variance

with the one-way analysis of variance. Then, a post hoc *t* test was performed. Significance level between sham IL/sham CL, sham IL/SNI IL, sham CL/SNI CL, and SNI IL/SNI CL were marked in the graphs with $*P < 0.05$; $**P < 0.01$; $***P < 0.001$.

Supplementary Table 2 (available at http://links.lww.com/PAIN/B704) shows all statistical values, including *P* values and Bonferroni-corrected *P* values (6 tests), of calculated image parameters. Data are presented as the mean ± standard error.

3. Results

3.1. Deep learning–based image segmentation enables analysis of a large dataset

To test whether the SNI model in rats is valid, we measured nocifensive behavior on several time points for up to 2 weeks. We observed mechanical and cold allodynia but no heat hyperalgesia 7 and 14 days after SNI surgery (Supplementary Fig. 1, available at http://links.lww.com/PAIN/B703). Likewise, initial qualitative assessment of the acquired immunofluorescence microscopy images was in line with previous studies: NF labelling showed sensory neuron somata as well as fiber-rich regions (**Fig. 1A**), and both GS and GFAP immunoreactivity formed ring-like image features, surrounding the NF-labeled sensory neuron somata. As expected, GFAP signals were more pronounced in DRG sections with SNI (**Fig. 1A and B**).

To objectively investigate SNI-induced changes in L4 and L5 rat DRG, we used a DL-based image segmentation approach described previously for brain tissue[19,56] (**Fig. 2**). We computed 2 DL model ensembles, one for the annotation of NF-positive neuronal somata and one for both GS-positive and GFAP-positive glial cells (**Fig. 2**). To increase objectivity, we used ground truth estimated annotations of 3 experts to train the DL models.[56] Eventually, this enabled us to automatically analyze a total of 2541 images of DRG sections (847 per marker). A measure for validity for segmentation purposes is the intersection over union (IoU) value. Intersection over union, an overlap metric, was used to measure how well expert annotations in single images overlap with estimated ground truth annotations, with 0 meaning no overlap and 1 meaning a perfect match. According to other studies, a mean IoU value of at least 0.50 indicates overlapping segmentations of 2 ROIs.[12,19,40] Notably, expert annotations of NF-positive image features showed higher similarities (mean IoU = 0.86) than annotations of GFAP- (mean IoU = 0.61) or GS-positive image features (mean IoU = 0.65), possibly because glial cells with ring-like structures were harder to percept or annotate (Supplementary Table 1, available at http://links.lww.com/PAIN/B703). Likewise, the NF model ensemble performed better than the GS/GFAP glial cell model ensemble. All models provide IoU values close to the performance of the human experts (Supplementary Figs. 2-4, available at http://links.lww.com/PAIN/B703). Moreover, all images and their predicted masks are provided online to show the performance of the models.[55]

3.2. Glial fibrillary acidic protein increase after spared nerve injury is reflected by integrated signal density in image feature segments

Because of high variance and regional difference in GFAP expression, as interactively visualized in our data app (https://share.streamlit.io/amschulte/drg/main), image analysis based on heuristic methods was problematic. The results would bias toward the image sections selected for manual analysis. To completely capture the DRG variability, we analyzed many serial DRG sections. One parameter that can easily be quantified for many images is the raw average fluorescence intensity. However, tissue sections were variable in having SGCs, GFAP did not exclusively stain SGCs (**Fig. 1**), and SGCs, being very small, flat cells,[48] have a small area compared with the rest of the tissue. Therefore, changes in the number of SGCs expressing GFAP could be obscured by average intensity. As a result, no significant changes were seen in mean raw average fluorescence intensity of GFAP or GS 14 days after injury (**Fig. 3A and B**). Next, we used GFAP and GS segmentations generated by our DL model ensemble to calculate the integrated density of the immunofluorescence signals in the image feature segments. Thus, the analysis was restricted to ring-shaped SGCs, and the area in addition to the intensity of the feature signals was also considered. With this analysis, GFAP but not GS signals were significantly increased ipsilaterally 14 d after SNI (**Fig. 3C and D**). Note that specifically the ring-like structures around neurons were annotated and thus recognized by the DL model ensemble (**Fig. 3E and F**).

3.3. Glial fibrillary acidic protein increase in satellite glial cells after spared nerve injury experimentally validates the deep learning approach

Next, we analyzed GFAP upregulation in more detail to substantiate that the DL-based strategy extracts biologically relevant information from large-field bioimages. The GS/GFAP DL model ensemble produced valid segmentation results with a mean IoU of 0.543 on the GFAP test images (Supplementary Fig. 2, available at http://links.lww.com/PAIN/B703). The parameter, percentage of neurons in proximity to GFAP-positive glial cells, assigned GFAP-positive SGCs to their corresponding neuron (**Fig. 4A**). The GFAP area per neuronal area increased after SNI and was larger 7 days after injury than 14 days after injury (**Fig. 4B**). The percentage of neurons in proximity to GFAP-positive cells increased 3-fold in 7 d SNI. On day 14, the effect was slightly lower (**Fig. 4C**). Interestingly, twice as many medium-sized and large compared with small neurons were in proximity to GFAP-positive glial cells after injury (**Fig. 4D and E**).

3.4. The number of neurons is unchanged by spared nerve injury

We then exploit the automatized, DL-based annotation of image features to its full potential and used our large-scale data set to analyze more controversial plasticity changes in the DRG. Based on the NF segmentations, we investigated if neuronal loss occurs after short-term nerve injury. The NF DL model ensemble produced valid NF segmentations (mean IoU of 0.867, **Fig. 5A**, Supplementary Fig. 3, available at http://links.lww.com/PAIN/B703). Fifty to 60% were nociceptive, thermosensitive, and itch-sensitive (small, $< 700\ \mu m^2$) and 40 to 50% were mechanoreceptive and proprioceptive neurons (medium-sized and large, $\geq 700\ \mu m^2$) with no significant changes seen after injury (**Fig. 5B–E**). To estimate the total number of neurons, the number of neurons per tissue area based on a thresholded NF staining was used (**Fig. 5F**). The neuronal number was not changed at day 14 after injury (**Fig. 5G**).

3.5. Glutamine synthetase immunoreactivity in satellite glial cells decreases after spared nerve injury

Next, we analyzed GS, a supposed stable SGC marker in rodents. The GS/GFAP DL model ensemble used for the

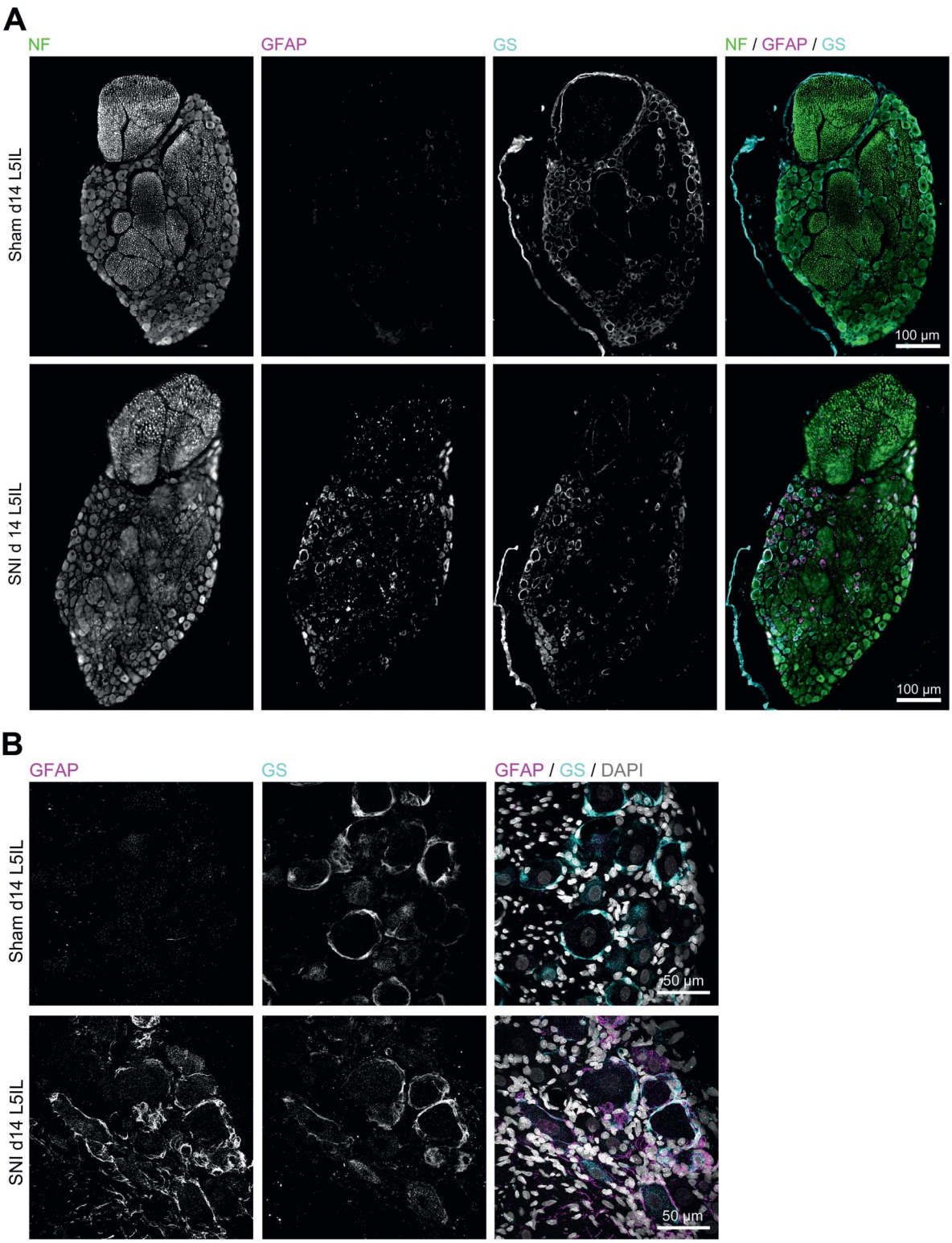

Figure 1. Increase of glial fibrillary acidic protein (GFAP) immunoreactivity in DRG after SNI. (A) Representative tile-scan images and (B) high-resolution confocal images display DRG sections from Wistar rats at 14 d after SNI or sham operation. Labelled are satellite glial cells (SGCs) using GFAP (magenta), glutamine synthetase (GS, cyan), and neurons using neurofilament (NF, green). DAPI (white) stains nuclei. (A) scale bar = 100 µm, B, scale bar = 50 µm). DRG, dorsal root ganglia; SNI, spared nerve injury.

segmentation of the GS images achieved a mean IoU of 0.583 on the test images (Supplementary Fig. 4, available at http://links.lww.com/PAIN/B703). The GS-positive area was analyzed like the GFAP-positive area (**Fig. 6A**). Surprisingly, the GS area and the percentage of neurons in proximity to GS-positive SGCs were decreased after SNI (**Fig. 6B and C**). Seven days after SNI, 15% less neurons were in proximity to GS-positive glial cells (**Fig. 6C**). Notably, the contralateral side also showed a small reduction in GS-positive glial cells, which was partly recovered 14 days after injury. Although more medium-sized and large neurons than small

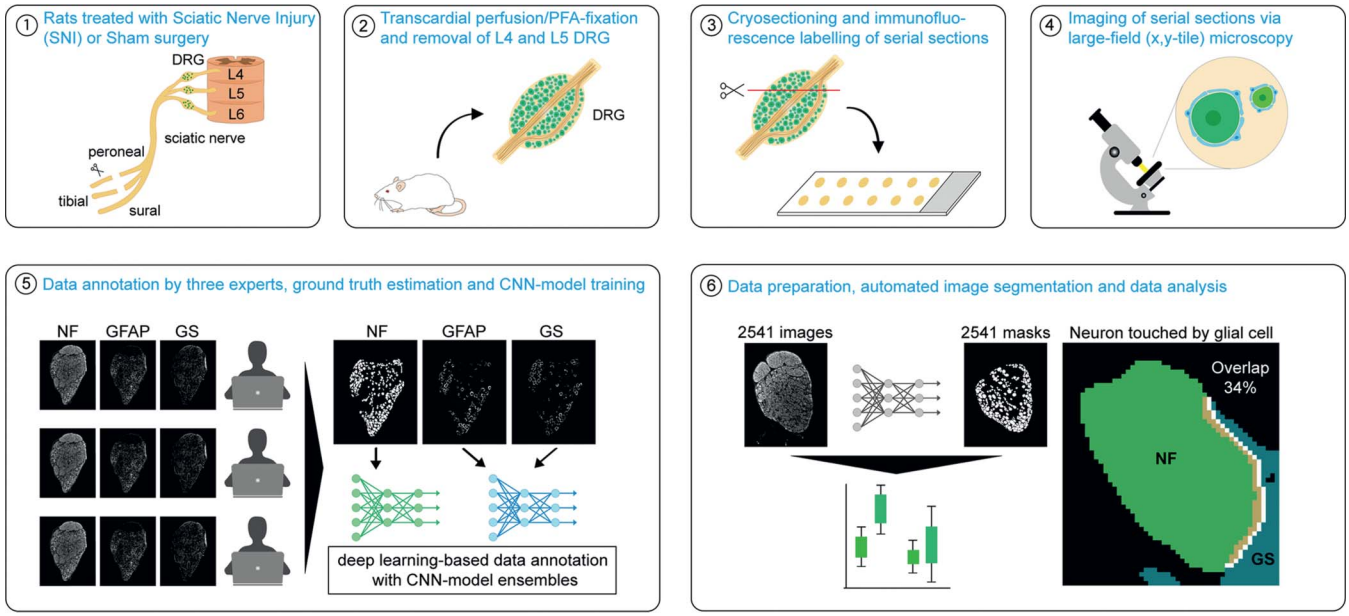

Figure 2. Schematic workflow and methods for systematic analysis of DRG in 6 steps. (1) Rats underwent SNI or sham surgery. (2) After 7 or 14 days, transcardial perfusion with the fixative PFA was performed and ipsilateral and contralateral L4/L5 DRG were removed. (3) Serial sections were cut collecting every 10th slice with a thickness of 16 μm on one slide. (4) DRG slices were labelled and imaged through large-field (tile) microscopy. (5) Three human experts annotated 15 representative microscopy images for each label according to their individual criteria. These data were used for computing a consensus for ground truth estimation; 80% of the data set were used to train deep learning (DL) model ensembles for NF, or GS and GFAP. 20% of the annotated images were used as the test data set. (6) Segmentation masks were predicted for a total of 2541 images. Based on these, quantification and statistical analyses were conducted. Changes in GS and GFAP levels were analyzed by quantifying the amount and size of neurons in proximity to GS-positive or GFAP-positive glial cells (overlap > 0%). DRG, dorsal root ganglia; GS, glutamine synthetase; GFAP, glial fibrillary acidic protein; SNI, spared nerve injury.

neurons were in proximity to GS-positive glial cells, a significant decrease in GS was seen for all neuronal sizes (**Fig. 6D and E**).

3.6. Satellite glial cells switch their phenotype

Because we saw more GFAP-positive but less GS-positive SGCs, we analyzed this phenotype switch more closely. Glial fibrillary acidic protein and GS segmentation were merged into one glial cell ring segmentation. As in the previous analysis, the area of the glial cell rings and the percentage of the neurons which are in proximity to SGCs were determined (**Fig. 7A**). Furthermore, the GS and GFAP segmentation overlap was analyzed relative to the GS or GFAP segmentation area, respectively (**Fig. 7B**).

We found a small significant reduction in glial cells after SNI using the markers GS and GFAP. The glial cell ring area per neuronal area was reduced at the contralateral side after SNI (**Fig. 7C**). Both the ipsilateral and contralateral sides showed a significant decrease in neurons in proximity to glial cells 7 days after SNI (**Fig. 7D**). Fourteen days after SNI, no change was seen.

Finally, we observed changes in the composition of the glial cell markers. More GS-positive glial cells also expressed GFAP after SNI at the ipsilateral side (**Fig. 7E**). In contrast, fewer of the GFAP-positive glial cells were also GS positive after SNI (**Fig. 7F**). Note that after SNI, L4 and L5 DRGs were affected to a similar extent because both DRG locations had mainly similar values in most parameters (Supplementary Fig. 5, available at http://links.lww.com/PAIN/B703).

All in all, we saw no sign of gliosis, but a slight decrease in the number of GS- and/or GFAP-positive glial cells after SNI. SGCs shifted from a mainly GS-positive phenotype to a more GFAP-positive and less GS-positive phenotype.

4. Discussion

In this study, we established and validated DL-based image segmentation for systematic analysis of cellular plasticity of DRG resident cells in a pain-related animal model. DL-based image segmentation was necessary and suited to systematically analyze a large-scale DRG bioimage data set objectively and with the required precision. The fully automatized, pixelwise segmentation approach allowed us to unravel phenotypic shifts in cell plasticity in the DRG after SNI. We show more GFAP-positive and less GS-positive cells around neurons, although no neuronal loss was seen, indicating high plasticity of activated SGCs in DRG after nerve injury.

Dorsal root ganglia sections are extremely heterogenous, depending on how many nerve fibers and neuronal cell bodies are in the sectional plane. Furthermore, size and shape are highly variable, rendering automatized image analysis ever more complex. To reduce the risk of subjectivity or other bias produced by manual selection of image regions, we investigated a data set where every 10th DRG section was imaged as a whole unit. This created a large-scale bioimage data set, with each image showing hundreds of single image features. Conventional methods, such as heuristic analysis by human experts and hard-coded algorithms, are not practical and conclusive to analyze this large amount of variable data. To our advantage, DL-based image segmentation not only led us analyze large volumes of image data but also provided the necessary level of feature annotation precision. Thus, biologically relevant effects could be detected, despite the heterogeneity of DRGs and the local staining variabilities. The quantification of a known injury effect—GFAP upregulation—further validated our method.[24,62]

A second advantage of our method is that higher objectivity is achieved using ground truth data. Here, several annotators label the same image set; of which, a consensus annotation—ground truth—is formed. Training several DL models, so-called model

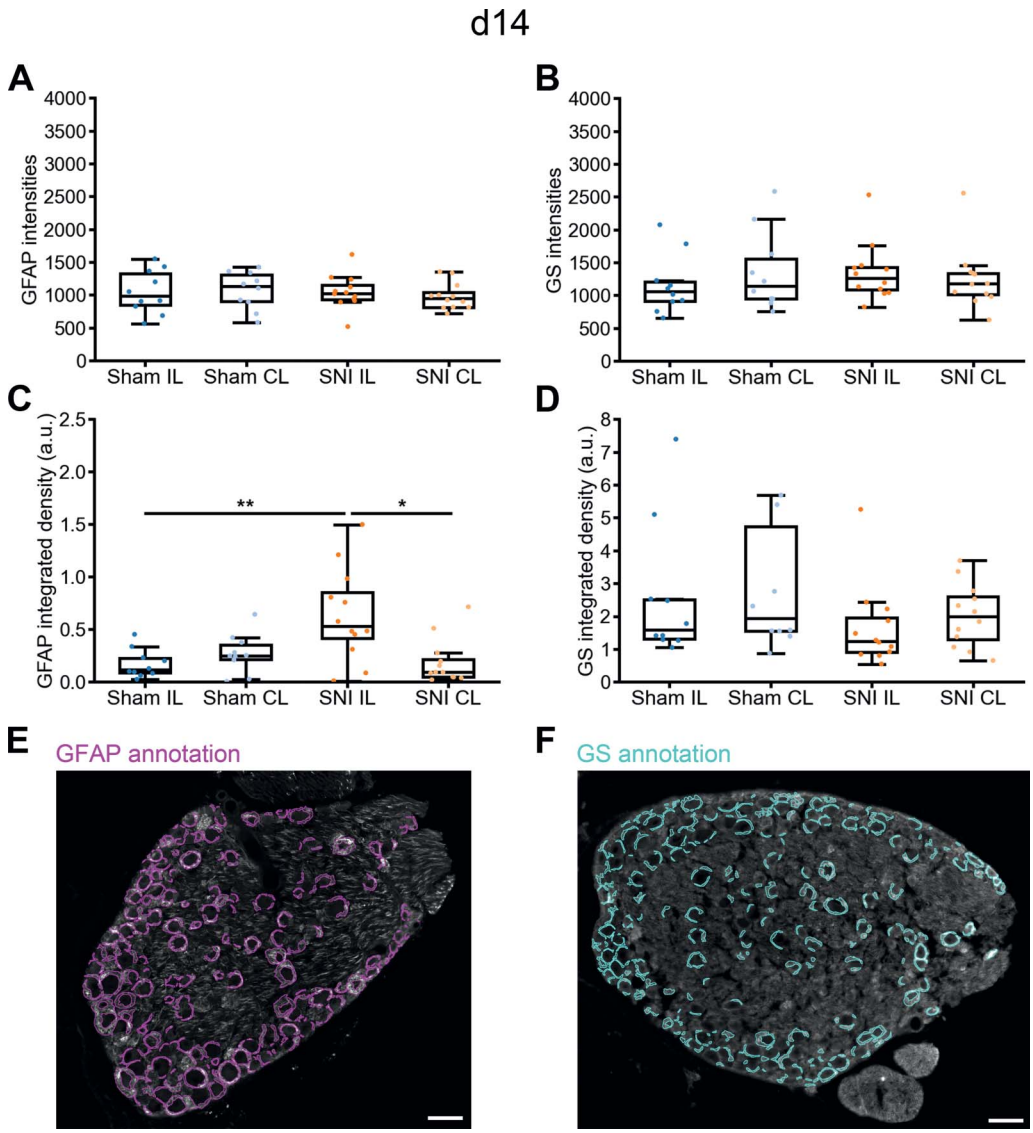

Figure 3. Unbiased DL-assisted image segmentation of GFAP after SNI. Rats were either treated by SNI or sham and analyzed 14 d after surgery. Mean raw GFAP or GS intensities of images (A and B) in comparison to integrated density of GFAP or GS images segmented with the DL model in arbitrary units (a.u.) (C and D). (E and F) Exemplary GFAP and GS annotations of one expert (scale bar = 100 μm). Depicted are sham ipsilateral (IL), sham contralateral (CL), SNI IL, and SNI CL (n = 10-12 DRG). Significant changes: $^{*}P \leq 0.05$; $^{**}P \leq 0.01$. DRG, dorsal root ganglia; GS, glutamine synthetase; GFAP, glial fibrillary acidic protein; SNI, spared nerve injury.

ensembles, further increase the validity and reliability of the results.[56] This allowed the NF, GS, and GFAP images to be segmented in sufficient quality for objective data analysis, as documented by the openly available data and by high segmentation quality test scores (intersection over union, IoU score), which are close to the human expert performance.

Third, our DL-based image analysis was able to evaluate several complex, for example, ring-like structures of SGCs, and variable structures (eg, GFAP after injury). Thus, we did not just quantify image features of low complexity, such as oval-shaped cells and nuclei, or signals with a high signal-to-noise ratio. The segmentation of GS-positive and GFAP-positive ring-like structures allowed us to quantify them in relation to each neuron. To define plasticity changes in the DRG, we introduced the parameter percentage of neurons in proximity to glial cells. This reflects the injury response of SGCs, but more important for this study, this can also be used as an objective plasticity parameter. The term underscores that neurons are functionally dependent on SGCs and within a very close distance of 20 nm to SGCs.[24] We are aware that a resolution of 0.908 μm/pixel in our large-field tile images cannot resolve such a distance; however, looking at the overlap of the one-pixel–dilated SGC and neuronal segmentations sufficiently quantified the cellular phenomenon. We showed that 38% of neurons are in proximity to GFAP-positive SGC 7 days after SNI, which is close to previously reported manually analyzed data.[44,62] 14 d after SNI, the value was lower (28%), suggesting that the GFAP injury response peaks at around 7 d after SNI. With our method, it is now possible to investigate whether SGC activation occurs specifically around injured neurons or whether SGC activation is a more global effect. For the approach here, injury-related GFAP upregulation was a highly effective marker for the visualization of injury responses. Notably, GFAP cannot serve as a universal marker for SGC reactivity because there are differences between species or experimental conditions.[43]

Spared nerve injury did not lead to neuronal death when analyzing the whole DRG. In previous studies, neuronal death

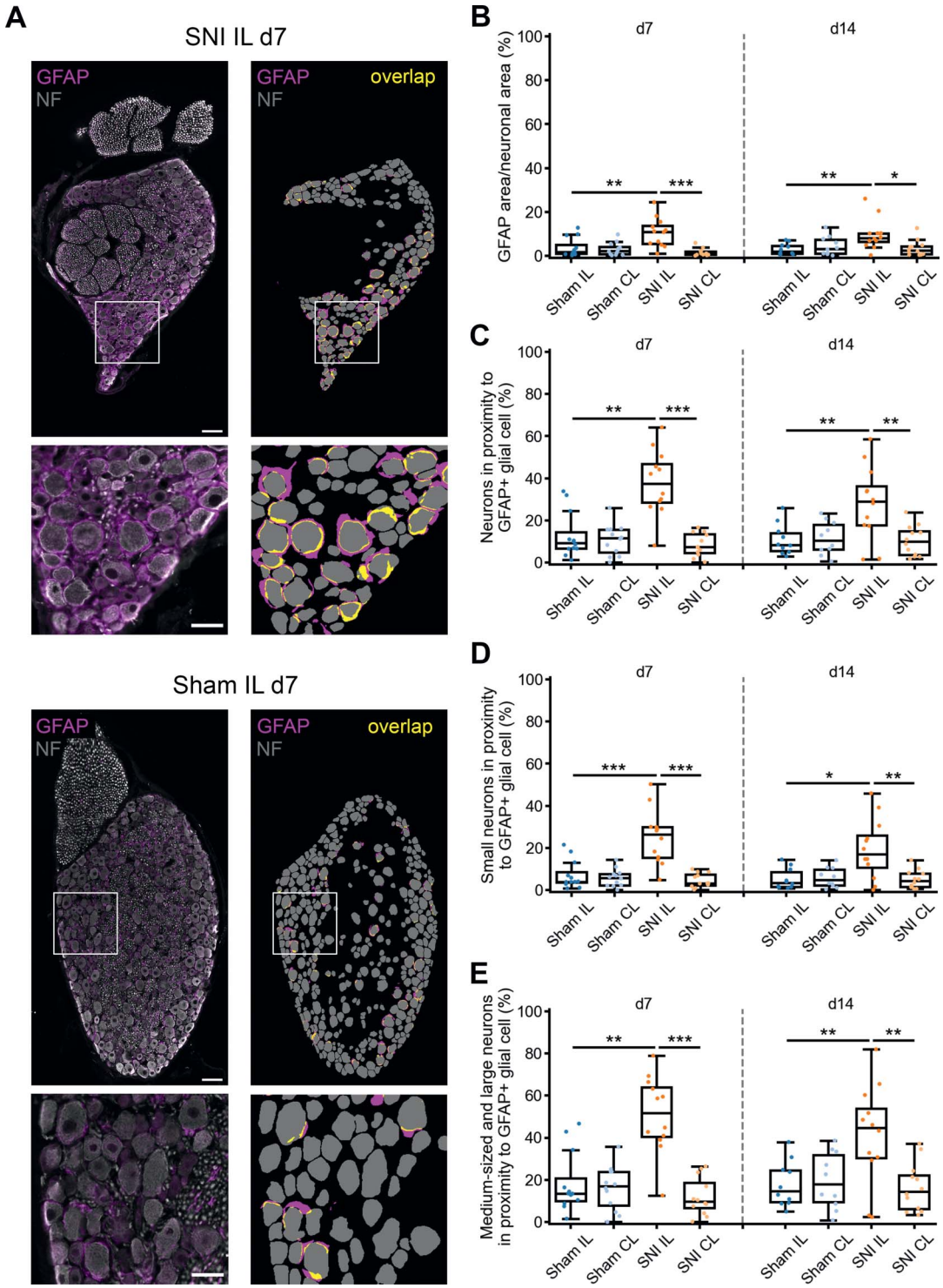

Figure 4. Increase in GFAP-positive SGCs around all types of neurons after SNI. (A) Representative immunofluorescent staining and corresponding DL-mediated segmentation of GFAP (magenta) and NF (gray) from SNI IL and sham IL injury sides. Yellow visualizes the overlap of GFAP-positive glial cells and neurons (scale bar = 100 μm/50 μm). (B–E) Image quantification displaying GFAP area per neuronal area (B, in %) as well as the percentage of all, small, and medium/large neurons that are in proximity to GFAP-positive glial cells. Sham IL, sham CL, SNI IL and SNI CL 7 d (left), and 14 d (right) after injury (n = 10-12 DRG) are shown. Significant changes: $^{*}P \leq 0.05$; $^{**}P \leq 0.01$; $^{***}P \leq 0.001$. DRG, dorsal root ganglia; GFAP, glial fibrillary acidic protein; SNI, spared nerve injury.

was observed after axotomy based on morphology and caspase-3 immunoreactivity.[33] In comparison, SNI was insufficient to induce neuronal cell death, possibly because not the whole nerve is damaged irreversibly. Size distributions of neurons were consistent with previously reported ones.[26,29,38,45] In addition, L4 and L5 DRG showed similar values in all measured parameters, indicating that SNI affects both DRG, consistent with observations of similar contributions of L4 and L5 spinal nerves to the sciatic nerve.[52,57]

Of particular interest was the phenotype switch of SGCs expressing GS and/or GFAP. Surprisingly, less GS-positive SGC were present after SNI. This could be a newly observed

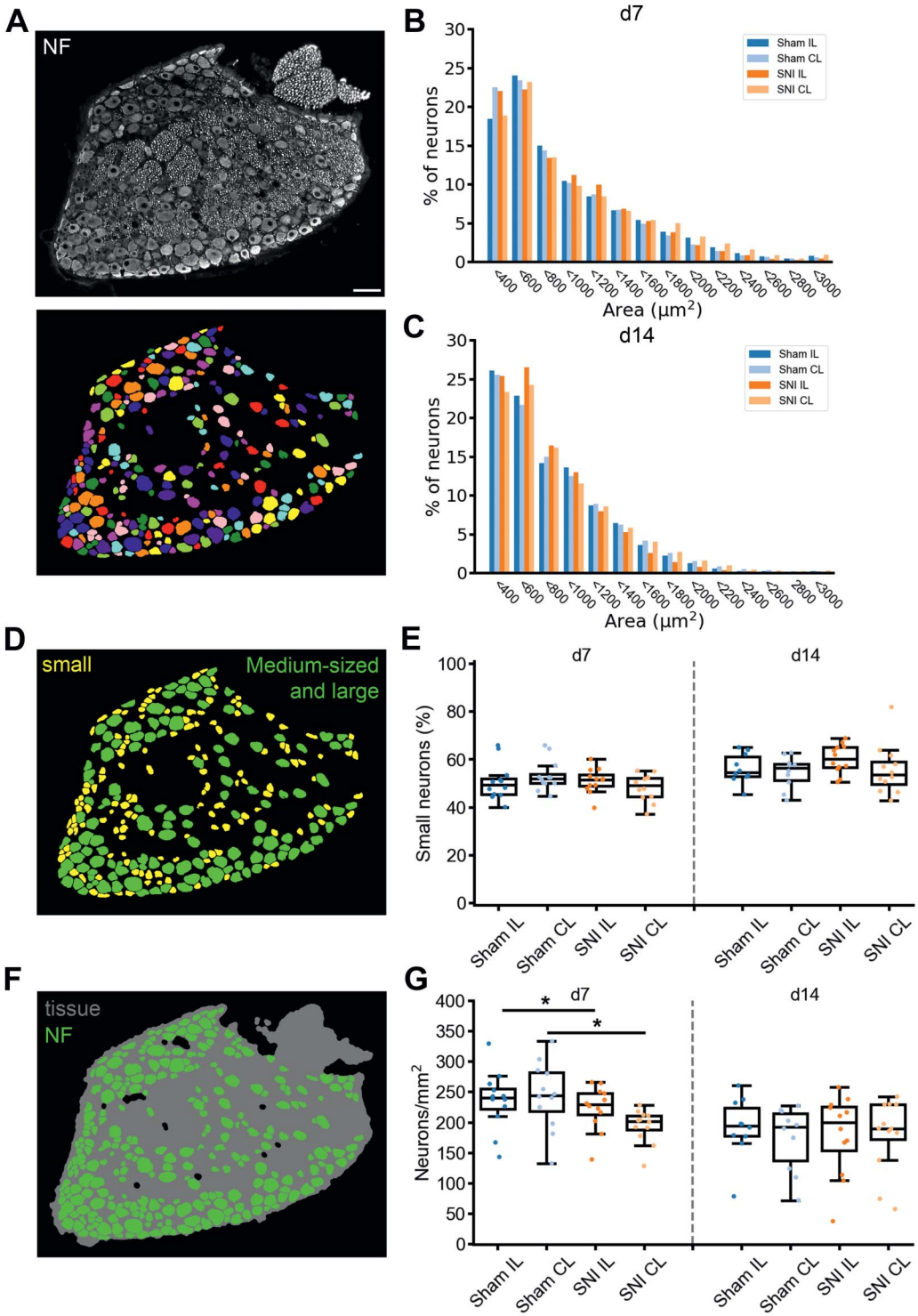

Figure 5. No loss of sensory neurons after SNI. (A) Segmentation of NF-stained DRG neurons (scale bar = 100 µm). (B and C) Size distribution of neurons 7 and 14 d after injury. (D and E) Relative number of small neurons (<700 µm^2) (yellow) and medium-sized and large neurons (green). (F and G) Visualization and quantification of cellular area including the number of neurons per square millimeter tissue area. Each dot represents the mean value of the images of one DRG from sham IL, sham CL, SNI IL, and SNI CL 7 d and 14 d after injury (n = 10-12). Significant changes: *$P \leq 0.05$. DRG, dorsal root ganglia; SNI, spared nerve injury.

downregulation of *Glul*, suggesting that GS expression is also modified in course of injury.[2,51] We saw no sign of gliosis after SNI using these markers, instead, even fewer GS-positive and/or GFAP-positive SGCs were detected around neurons. The area of GS/GFAP-positive glial cells was only smaller on the contralateral control side, which suggests that the overall SGC number is not changed. Nonetheless, we show that not all GFAP-positive glial cells are GS positive (59% in sham condition), confirming that not all SGCs are GS positive.[1,3] After SNI, 3 different phenotypes were quantified: (1) GS-positive SGCs with GFAP expression, (2) GS-positive but GFAP-negative SGCs, and (3) GFAP-positive but GS-negative SGCs.

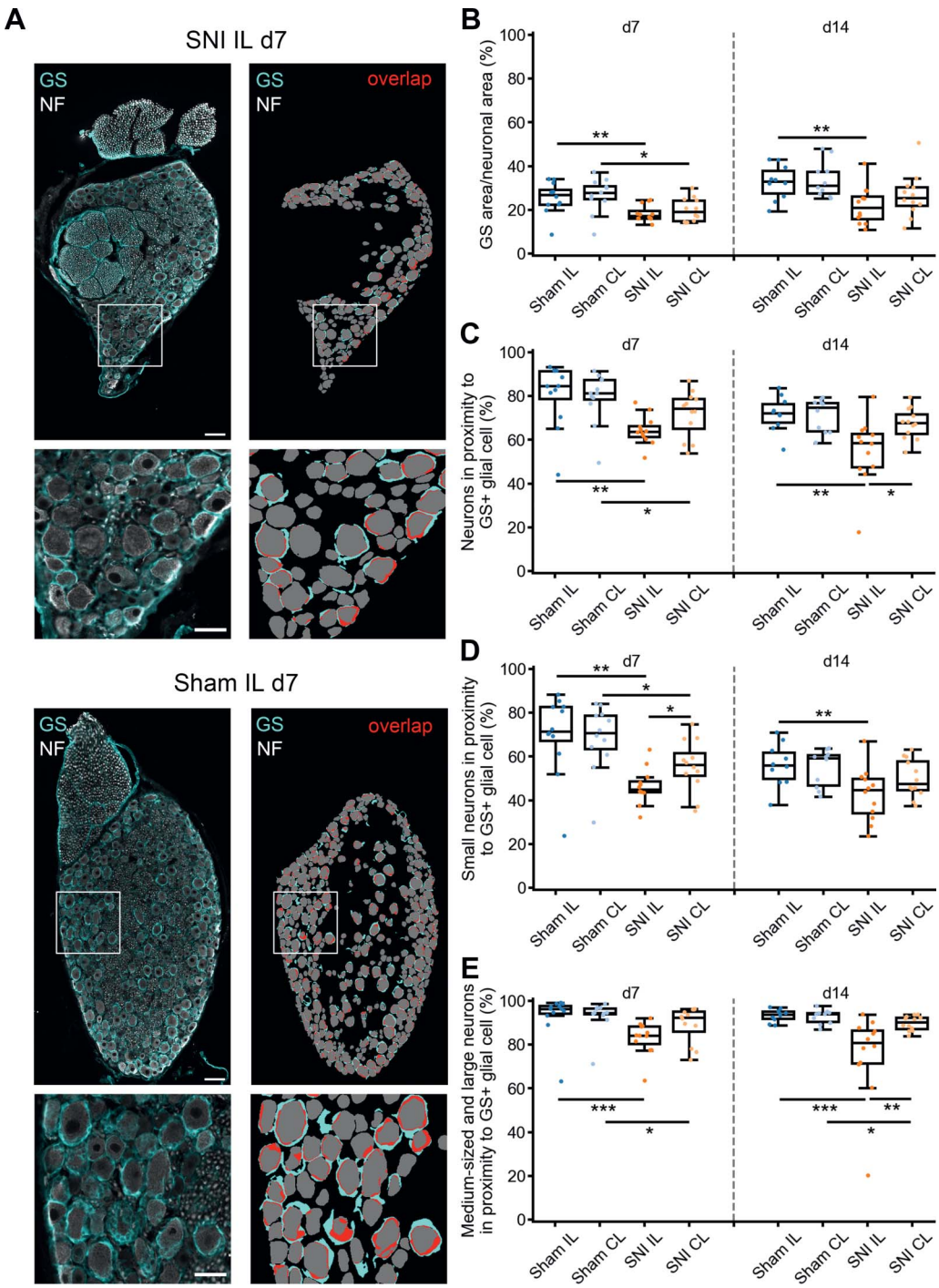

Figure 6. Decrease in GS-positive SGCs after SNI. (A) Exemplary images of immunofluorescent staining and corresponding segmentation of GS (cyan) and NF (gray) from SNI IL and sham IL injury sides, where red visualizes the overlap of GS-positive glial cells and neurons (scale bar = 100 μm/50 μm) (B) GS area per neuronal area (in %). (C–E) Percentage of all, small, medium-sized, and large neurons that are in proximity to GS-positive glial cells. Depicted are sham IL, sham CL, SNI IL, and SNI CL 7 d (left) and 14 d (right) after injury (n = 10-12 DRG). Significant changes are marked with: *$P \leq 0.05$; **$P \leq 0.01$; ***$P \leq 0.001$. DRG, dorsal root ganglia; GS, glutamine synthetase; SNI, spared nerve injury.

It is important to consider that GFAP is not only a pure marker for SGC reactivation,[11] but it is also expressed in progenitor cells and immature Schwann cells.[28,31] A dedifferentiation response of SGCs, as indicated by GFAP upregulation, could be interesting as a starting point for regenerative medicine. Notably, SGCs, derived from the neural crest like Schwann cells and DRG neurons, undergo dedifferentiation in vitro and exhibit a progenitor potential toward Schwann cells.[18] This suggests that SGCs might represent a population of Schwann cell precursors whose further development has been arrested in their specific in vivo microenvironment.[18]

Observed plasticity changes of SGCs are less pronounced 14 d after SNI compared with 7 d. We did not investigate whether and how observed plasticity changes affect mechanical allodynia. Therefore, we are not able to tell how the recovery of cellular parameters correlates with pain sensitivity changes. Animals

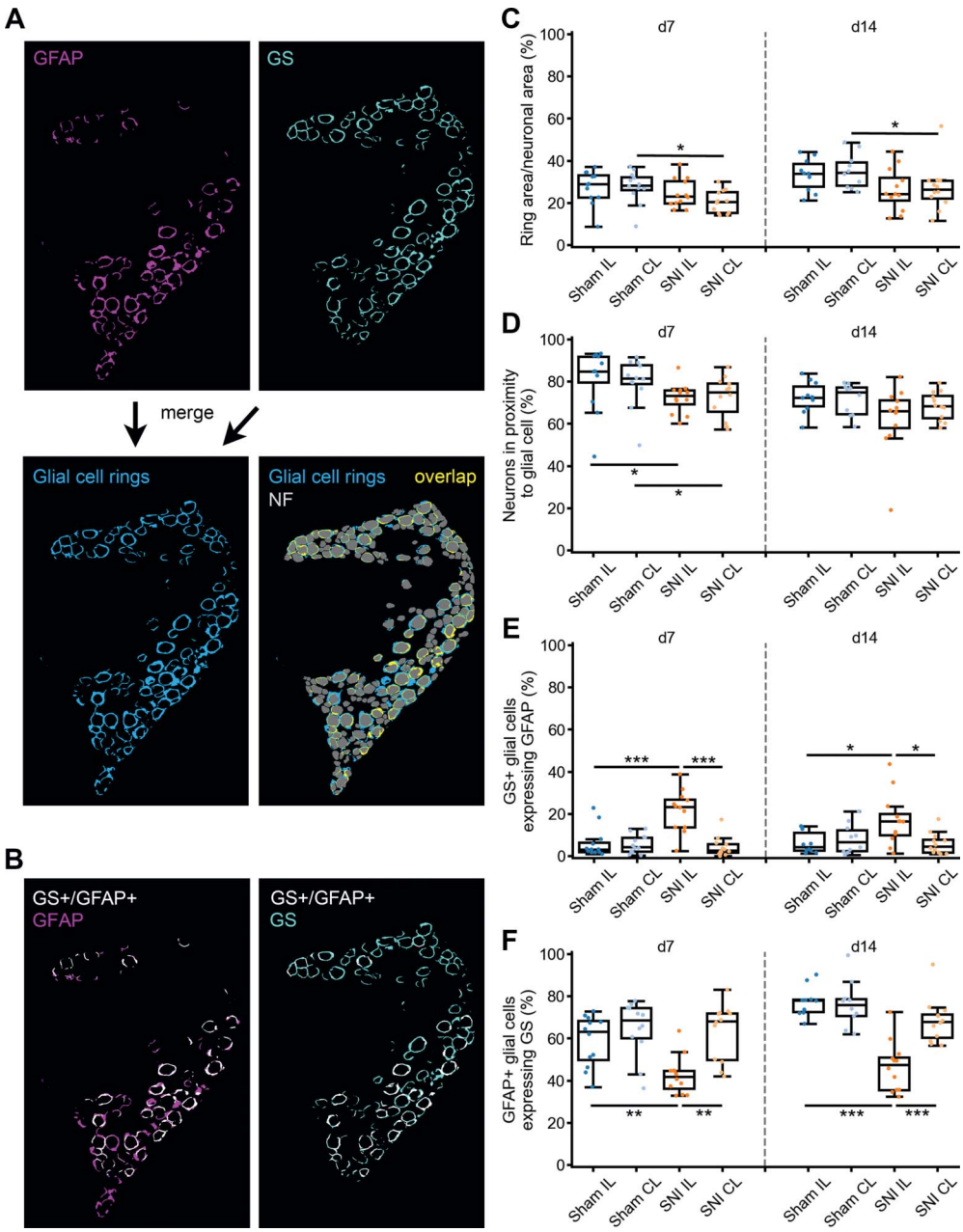

Figure 7. Cellular plasticity of SGCs after SNI. (A) Visualization of image analysis. GFAP (magenta) and GS (cyan) segmentation are merged into a glial cell ring segmentation (blue). NF-positive neurons that overlap with glial cell rings (yellow) are "neurons in proximity to glial cells". (B) The overlap of GS-positive and GFAP-positive glial cells (white) was quantified in relation to all GFAP-positive (magenta + white) or GS-positive (cyan + white) glial cells. Image quantification for glial cell ring area per neuronal area (C), neurons in proximity to glial cells (D), as well as GS-positive glial cells expressing GFAP-positive (E), and GFAP-positive glial cells expressing GS (F) are shown (in %). Compared with sham IL, sham CL, SNI IL, and SNI CL 7 d (left) and 14 d (right) after injury (n = 10-12 DRG). Significant changes: $^{*}P \leq 0.05$; $^{**}P \leq 0.01$; $^{***}P \leq 0.001$. DRG, dorsal root ganglia; GS, glutamine synthetase; GFAP, glial fibrillary acidic protein; SNI, spared nerve injury.

develop robust allodynia and pain-like behavior that last for months after the tibioperoneal nerves are cut at SNI.[16,20,59] In line with other studies,[17,27,32,37,65] we focused on early plasticity responses (7, 14 days) after nerve injury. Early responses are also observed in injury models of the central nervous system. For instance, in the cortex of the mouse, reactive gliosis, GFAP upregulation, and glial phenotype changes are already detectable 1 day post lesion and are fully pronounced 7 days post lesion.[7] Surprisingly, we could not find evidence for pronounced cell death, loss of neuron–SGC entities, or gliosis in our SNI model. However, we cannot exclude that neuronal death and reactive gliosis occur at later time points after injury, eg, after months.

This study serves as an example of how DL-based bioimage data analysis can be applied in pain research. These data are useful reference for future studies looking at plasticity responses at later time points and in other pain models, as well as for retrospective reanalysis of open data and reevaluation of our results by others (reproducibility). Critical could be that, up to now, programming and data management skills are required for data analysis. To open the method to more users, we made our data set and analysis script openly available.[55] Availability and easy access to the raw data, analysis scripts, and DL models are important to allow DL model evolution in an open science community. Still, computational expertise is of advantage

because there is no one for all solution for complex bioimage analysis studies.

In summary, DL-based image segmentation enabled us to study cellular plasticity in DRG—the major relay station in the pain pathway—on the next level. Large-scale image analysis with DL had the advantages of being fully transparent, more objective, better scalable, and more specific about area size and location. Segmentation of thousands of entities of SGC rings and sensory neurons shows no injury-related loss of these cells within 14 days after spared nerve injury. Instead, SGC plasticity, in close proximity and possibly communication with its neuron, was visualized.

Conflict of interest statement

The authors have no conflicts of interest to declare.

Acknowledgments

The authors sincerely thank Matthias Griebel and Christoph M. Flath from the Department of Business and Economics at the University of Würzburg, Germany for their technical support with deepflash2. This work was funded by the Evangelisches Studienwerk Villigst (AS), the Interdisciplinary Center for Clinical Research Würzburg (IZKF) project N-D-368 (AA, RB, and HR), as well as by the Deutsche Forschungsgemeinschaft (DFG, German Research Foundation), project ID: 426503586, KFO5001 ResolvePAIN.
Data and materials availability: Images and corresponding segmentation as well as the DL models are open access[55] and exemplary image sets of rats 7 d after SNI and sham are visualized at: https://share.streamlit.io/amschulte/drg/main. The python scripts of the analysis are openly available on GitHub: https://github.com/AmSchulte/DRG.
Author contributions: Conceptualization: A. Aue, A. Schulte, H.L. Rittner, R. Blum; Methodology: A. Aue, A. Schulte, J. Degenbeck, H. Lohner, R. Blum; Investigation: A. Aue, A. Schulte, J. Degenbeck, H. Lohner; Software: A. Schulte; Formal analysis: A. Aue, A. Schulte; Funding acquisition: H.L. Rittner, R. Blum, A. Schulte; Supervision: H.L. Rittner, R. Blum, A. Aue; Project administration: H.L. Rittner, R. Blum; Writing—original draft: A. Aue, A. Schulte; Writing—review & editing: A. Aue, A. Schulte, H.L. Rittner, R. Blum.

Appendix A. Supplemental digital content

Supplemental digital content associated with this article can be found online at http://links.lww.com/PAIN/B703 and http://links.lww.com/PAIN/B704.

Article history:
Received 4 June 2022
Received in revised form 13 July 2022
Accepted 26 July 2022
Available online 15 August 2022

References

[1] Avraham O, Chamessian A, Feng R, Halevi AE, Moore AM, Gereau RW, Cavalli V. Profiling the molecular signature of satellite glial cells at the single cell level reveals high similarities between rodent and human. PAIN 2022;163:2348-64.
[2] Avraham O, Deng P-Y, Jones S, Kuruvilla R, Semenkovich CF, Klyachko VA, Cavalli V. Satellite glial cells promote regenerative growth in sensory neurons. Nat Commun 2020;11:4891.
[3] Avraham O, Feng R, Ewan EE, Rustenhoven J, Zhao G, Cavalli V. Profiling sensory neuron microenvironment after peripheral and central axon injury reveals key pathways for neural repair. eLife 2021;10:e68457.
[4] Ben-Kraiem A, Sauer RS, Norwig C, Popp M, Bettenhausen AL, Atalla MS, Brack A, Blum R, Doppler K, Rittner HL. Selective blood-nerve barrier leakiness with claudin-1 and vessel-associated macrophage loss in diabetic polyneuropathy. J Mol Med (Berl) 2021;99:1237–50.
[5] Boateng EK, Novejarque A, Pheby T, Rice ASC, Huang W. Heterogeneous responses of dorsal root ganglion neurons in neuropathies induced by peripheral nerve trauma and the antiretroviral drug stavudine. Eur J Pain 2015;19:236–45.
[6] Bourquin A-F, Süveges M, Pertin M, Gilliard N, Sardy S, Davison AC, Spahn DR, Decosterd I. Assessment and analysis of mechanical allodynia-like behavior induced by spared nerve injury (SNI) in the mouse. PAIN 2006;122:14e11–14e14.
[7] Buffo A, Rite I, Tripathi P, Lepier A, Colak D, Horn AP, Mori T, Gotz M. Origin and progeny of reactive gliosis: a source of multipotent cells in the injured brain. Proc Natl Acad Sci United States America 2008;105:3581–6.
[8] Chaplan SR, Bach FW, Pogrel JW, Chung JM, Yaksh TL. Quantitative assessment of tactile allodynia in the rat paw. J Neurosci Methods 1994;53:55–63.
[9] Decosterd I, Woolf CJ. Spared nerve injury: an animal model of persistent peripheral neuropathic pain. PAIN 2000;87:149–58.
[10] Deuis JR, Dvorakova LS, Vetter I. Methods used to evaluate pain behaviors in rodents. Front Mol Neurosci 2017;10:284.
[11] Escartin C, Galea E, Lakatos A, O'Callaghan JP, Petzold GC, Serrano-Pozo A, Steinhäuser C, Volterra A, Carmignoto G, Agarwal A, Allen NJ, Araque A, Barbeito L, Barzilai A, Bergles DE, Bonvento G, Butt AM, Chen W-T, Cohen-Salmon M, Cunningham C, Deneen B, De Strooper B, Díaz-Castro B, Farina C, Freeman M, Gallo V, Goldman JE, Goldman SA, Götz M, Gutiérrez A, Haydon PG, Heiland DH, Hol EM, Holt MG, Iino M, Kastanenka KV, Kettenmann H, Khakh BS, Koizumi S, Lee CJ, Liddelow SA, MacVicar BA, Magistretti P, Messing A, Mishra A, Molofsky AV, Murai KK, Norris CM, Okada S, Oliet SHR, Oliveira JF, Panatier A, Parpura V, Pekna M, Pekny M, Pellerin L, Perea G, Pérez-Nievas BG, Pfrieger FW, Poskanzer KE, Quintana FJ, Ransohoff RM, Riquelme-Perez M, Robel S, Rose CR, Rothstein JD, Rouach N, Rowitch DH, Semyanov A, Sirko S, Sontheimer H, Swanson RA, Vitorica J, Wanner I-B, Wood LB, Wu J, Zheng B, Zimmer ER, Zorec R, Sofroniew MV, Verkhratsky A. Reactive astrocyte nomenclature, definitions, and future directions. Nat Neurosci 2021;24:312–25.
[12] Falk T, Mai D, Bensch R, Cicek O, Abdulkadir A, Marrakchi Y, Bohm A, Deubner J, Jackel Z, Seiwald K, Dovzhenko A, Tietz O, Dal Bosco C, Walsh S, Saltukoglu D, Tay TL, Prinz M, Palme K, Simons M, Diester I, Brox T, Ronneberger O. U-Net: deep learning for cell counting, detection, and morphometry. Nat Methods 2019;16:67–70.
[13] Flatters SJ, Bennett GJ. Ethosuximide reverses paclitaxel- and vincristine-induced painful peripheral neuropathy. Pain 2004;109:150–61.
[14] Gage GJ, Kipke DR, Shain W. Whole animal perfusion fixation for rodents. J Vis Exp 2012;65:3564.
[15] Gallaher ZR, Johnston ST, Czaja K. Neural proliferation in the dorsal root ganglia of the adult rat following capsaicin-induced neuronal death. J Comp Neurol 2014;522:3295–307.
[16] Gangadharan V, Zheng H, Taberner FJ, Landry J, Nees TA, Pistolic J, Agarwal N, Mannich D, Benes V, Helmstaedter M, Ommer B, Lechner SG, Kuner T, Kuner R. Neuropathic pain caused by miswiring and abnormal end organ targeting. Nature 2022;606:137–45.
[17] Gehrmann J, Monaco S, Kreutzberg GW. Spinal cord microglial cells and DRG satellite cells rapidly respond to transection of the rat sciatic nerve. Restorative Neurol Neurosci 1991;2:181–98.
[18] George D, Ahrens P, Lambert S. Satellite glial cells represent a population of developmentally arrested Schwann cells. Glia 2018;66:1496–506.
[19] Griebel M, Segebarth D, Stein N, Schukraft N, Tovote P, Blum R, Flath CM. Deep-learning in the bioimaging wild: Handling ambiguous data with deepflash2. ArXiv 2021;abs/2111.06693.
[20] Guida F, Iannotta M, Misso G, Ricciardi F, Boccella S, Tirino V, Falco M, Desiderio V, Infantino R, Pieretti G, de Novellis V, Papaccio G, Luongo L, Caraglia M, Maione S. Long-term neuropathic pain behaviors correlate with synaptic plasticity and limbic circuit alteration: a comparative observational study in mice. PAIN 2022;163:1590-1602.
[21] Haberberger RV, Barry C, Dominguez N, Matusica D. Human dorsal root ganglia. Front Cell Neurosci 2019;13:271.
[22] Hackel D, Brack A, Fromm M, Rittner HL. Modulation of tight junction proteins in the perineurium for regional pain control. Ann New York Acad Sci 2012;1257:199–206.

[23] Hanani M. Satellite glial cells in sensory ganglia: from form to function. Brain Res Rev 2005;48:457–76.
[24] Hanani M, Spray DC. Emerging importance of satellite glia in nervous system function and dysfunction. Nat Rev Neurosci 2020;21:485–98.
[25] Hargreaves K, Dubner R, Brown F, Flores C, Joris J. A new and sensitive method for measuring thermal nociception in cutaneous hyperalgesia. PAIN 1988;32:77–88.
[26] Harper AA, Lawson SN. Conduction velocity is related to morphological cell type in rat dorsal root ganglion neurones. J Physiol 1985;359:31–46.
[27] Jager SE, Pallesen LT, Richner M, Harley P, Hore Z, McMahon S, Denk F, Vægter CB. Changes in the transcriptional fingerprint of satellite glial cells following peripheral nerve injury. Glia 2020;68:1375–95.
[28] Jessen KR, Mirsky R. The origin and development of glial cells in peripheral nerves. Nat Rev Neurosci 2005;6:671–82.
[29] Kamiya H, Zhang W, Sima AAF. Degeneration of the Golgi and neuronal loss in dorsal root ganglia in diabetic BioBreeding/Worcester rats. Diabetologia 2006;49:2763–74.
[30] Kim YS, Anderson M, Park K, Zheng Q, Agarwal A, Gong C, Saijilafu YL, He S, LaVinka PC, Zhou F, Bergles D, Hanani M, Guan Y, Spray DC, Dong X. Coupled activation of primary sensory neurons contributes to chronic pain. Neuron 2016;91:1085–96.
[31] Kriegstein A, Alvarez-Buylla A. The glial nature of embryonic and adult neural stem cells. Annu Rev Neurosci 2009;32:149–84.
[32] Krishnan A, Bhavanam S, Zochodne D. An intimate role for adult dorsal root ganglia resident cycling cells in the generation of local macrophages and satellite glial cells. J Neuropathol Exp Neurol 2018;77:929–41.
[33] Kuo LT, Simpson A, Schanzer A, Tse J, An SF, Scaravilli F, Groves MJ. Effects of systemically administered NT-3 on sensory neuron loss and nestin expression following axotomy. J Comp Neurol 2005;482:320–32.
[34] Laine RF, Arganda-Carreras I, Henriques R, Jacquemet G. Avoiding a replication crisis in deep-learning-based bioimage analysis. Nat Methods 2021;18:1136–44.
[35] Li CH, Tam PKS. An iterative algorithm for minimum cross entropy thresholding. Pattern Recognition Lett 1998;19:771–6.
[36] Lim H, Lee H, Noh K, Lee SJ. IKK/NF-κB-dependent satellite glia activation induces spinal cord microglia activation and neuropathic pain after nerve injury. PAIN 2017;158:1666–77.
[37] Liu F-Y, Sun Y-N, Wang F-T, Li Q, Su L, Zhao Z-F, Meng X-L, Zhao H, Wu X, Sun Q, Xing G-G, Wan Y. Activation of satellite glial cells in lumbar dorsal root ganglia contributes to neuropathic pain after spinal nerve ligation. Brain Res 2012;1427:65–77.
[38] Lu S-G, Zhang X, Gold MS. Intracellular calcium regulation among subpopulations of rat dorsal root ganglion neurons. J Physiol 2006;577:169–90.
[39] Lucas AM, Ryder PV, Li B, Cimini BA, Eliceiri KW, Carpenter AE. Open-source deep-learning software for bioimage segmentation. Mol Biol Cell 2021;32:823–9.
[40] Maška M, Ulman V, Svoboda D, Matula P, Ederra C, Urbiola A, España T, Venkatesan S, Balak DM, Karas P, Bolcková T, Streitová M, Carthel C, Coraluppi S, Harder N, Rohr K, Magnusson KE, Jaldén J, Blau HM, Dzyubachyk O, Křížek P, Hagen GM, Pastor-Escuredo D, Jimenez-Carretero D, Ledesma-Carbayo MJ, Muñoz-Barrutia A, Meijering E, Kozubek M, Ortiz-de-Solorzano C. A benchmark for comparison of cell tracking algorithms. Bioinformatics 2014;30:1609–17.
[41] Miller KE, Richards BA, Kriebel RM. Glutamine-, glutamine synthetase-, glutamate dehydrogenase- and pyruvate carboxylase-immunoreactivities in the rat dorsal root ganglion and peripheral nerve. Brain Res 2002;945:202–11.
[42] Moen E, Bannon D, Kudo T, Graf W, Covert M, Van Valen D. Deep learning for cellular image analysis. Nat Methods 2019;16:1233–46.
[43] Mohr KM, Pallesen LT, Richner M, Vaegter CB. Discrepancy in the usage of GFAP as a marker of satellite glial cell reactivity. Biomedicines 2021;9:1022.
[44] Noh M-c, Mikler B, Joy T, Smith PA. Time course of inflammation in dorsal root ganglia correlates with differential reversibility of mechanical allodynia. Neuroscience 2020;428:199–216.
[45] Novakovic SD, Tzoumaka E, McGivern JG, Haraguchi M, Sangameswaran L, Gogas KR, Eglen RM, Hunter JC. Distribution of the tetrodotoxin-resistant sodium channel PN3 in rat sensory neurons in normal and neuropathic conditions. J Neurosci 1998;18:2174–87.
[46] Ogawa R, Fujita K, Ito K. Mouse embryonic dorsal root ganglia contain pluripotent stem cells that show features similar to embryonic stem cells and induced pluripotent stem cells. Biol open 2017;6:602–18.
[47] Ohara PT, Vit J-P, Bhargava A, Jasmin L. Evidence for a role of connexin 43 in trigeminal pain using RNA interference in vivo. J Neurophysiol 2008;100:3064–73.
[48] Pannese E. The satellite cells of the sensory ganglia. Adv Anat Embryol Cell Biol 1981;65:1–111.
[49] Pannese E. The structure of the perineuronal sheath of satellite glial cells (SGCs) in sensory ganglia. Neuron Glia Biol 2010;6:3–10.
[50] Reinhold AK, Yang S, Chen JTC, Hu L, Sauer RS, Krug SM, Mambretti EM, Fromm M, Brack A, Rittner HL. Tissue plasminogen activator and neuropathy open the blood-nerve barrier with upregulation of microRNA-155-5p in male rats. Biochim Biophys Acta (Bba) Mol Basis Dis 2019;1865:1160–9.
[51] Renthal W, Tochitsky I, Yang L, Cheng YC, Li E, Kawaguchi R, Geschwind DH, Woolf CJ. Transcriptional reprogramming of distinct peripheral sensory neuron subtypes after axonal injury. Neuron 2020;108:128–44. e129.
[52] Rigaud M, Gemes G, Barabas ME, Chernoff DI, Abram SE, Stucky CL, Hogan QH. Species and strain differences in rodent sciatic nerve anatomy: implications for studies of neuropathic pain. PAIN 2008;136:188–201.
[53] Sauer R-S, Kirchner J, Yang S, Hu L, Leinders M, Sommer C, Brack A, Rittner HL. Blood–spinal cord barrier breakdown and pericyte deficiency in peripheral neuropathy. Ann New York Acad Sci 2017;1405:71–88.
[54] Schneider CA, Rasband WS, Eliceiri KW. NIH Image to ImageJ: 25 years of image analysis. Nat Methods 2012;9:671–5.
[55] Schulte A, Lohner H, Degenbeck J, Segebarth D, Rittner H, Blum R, Aue A. Data from: Unbiased analysis of cellular plasticity in the dorsal root ganglion after peripheral nerve injury. Zenodo, 2022.
[56] Segebarth D, Griebel M, Stein N, von Collenberg CR, Martin C, Fiedler D, Comeras LB, Sah A, Schoeffler V, Lüffe T, Dürr A, Gupta R, Sasi M, Lillesaar C, Lange MD, Tasan RO, Singewald N, Pape HC, Flath CM, Blum R. On the objectivity, reliability, and validity of deep learning enabled bioimage analyses. eLife 2020;9:e59780.
[57] Swett JE, Torigoe Y, Elie VR, Bourassa CM, Miller PG. Sensory neurons of the rat sciatic nerve. Exp Neurol 1991;114:82–103.
[58] Takeda M, Takahashi M, Matsumoto S. Contribution of the activation of satellite glia in sensory ganglia to pathological pain. Neurosci Biobehavioral Rev 2009;33:784–92.
[59] Topham L, Gregoire S, Kang H, Salmon-Divon M, Lax E, Millecamps M, Szyf M, Stone LS. The transition from acute to chronic pain: dynamic epigenetic reprogramming of the mouse prefrontal cortex up to 1 year after nerve injury. PAIN 2020;161:2394–409.
[60] Warwick RA, Hanani M. The contribution of satellite glial cells to chemotherapy-induced neuropathic pain. Eur J Pain 2013;17:571–80.
[61] Woodham P, Anderson PN, Nadim W, Turmaine M. Satellite cells surrounding axotomised rat dorsal root ganglion cells increase expression of a GFAP-like protein. Neurosci Lett 1989;98:8–12.
[62] Xie W, Strong JA, Zhang JM. Early blockade of injured primary sensory afferents reduces glial cell activation in two rat neuropathic pain models. Neuroscience 2009;160:847–57.
[63] Xu M, Aita M, Chavkin C. Partial infraorbital nerve ligation as a model of trigeminal nerve injury in the mouse: behavioral, neural, and glial reactions. The J Pain 2008;9:1036–48.
[64] Yoon C, Wook YY, Sik NH, Ho KS, Mo CJ. Behavioral signs of ongoing pain and cold allodynia in a rat model of neuropathic pain. PAIN 1994;59.
[65] Yuan Q, Liu X, Xian YF, Yao M, Zhang X, Huang P, Wu W, Lin ZX. Satellite glia activation in dorsal root ganglion contributes to mechanical allodynia after selective motor fiber injury in adult rats. Biomed Pharmacother 2020;127:110187.